Quaternary Geochronology 85 (2024) 101630

Contents lists available at ScienceDirect

Quaternary Geochronology

journal homepage: www.elsevier.com/locate/quageo

Luminescence dating of rock surfaces in challenging environments: The case of MIS5e gravelly transgressive lag deposit (Southern Sardinia, West Mediterranean Sea)

Giulia Cossu [a,*], Daniele Sechi [a,d], Reza Sohbati [b], Andrew Murray [c], Vincenzo Pascucci [a], Stefano Andreucci [d]

[a] Department of Architecture, Design and Planning, University of Sassari, Piazza Duomo 6, I-07041, Alghero (SS), Italy
[b] Department of Physics, Technical University of Denmark, DTU Risø Campus, DK-4000, Roskilde, Denmark
[c] Department of Geoscience, Aarhus University, Risø Campus, DK-4000, Roskilde, Denmark
[d] Dipartimento di Scienze Chimiche e Geologiche, Università degli Studi di Cagliari, Cittadella Universitaria (Blocco A), Monserrato, 09127, CA, Italy

ARTICLE INFO

Keywords:
Gravelly transgressive lag
Rock surface dating
Luminescence
Bleaching

ABSTRACT

Determining the age of precise sea level markers such as marine terraces is often difficult because of the inherent limitation of traditional dating methods. A novel method based on Optical Stimulated Luminescence applicable to rock surfaces has been showing great promise in dating boulder and cobble surfaces from various environments. We performed Optically Stimulated Luminescence Rock Surface Dating (OSL RSD) on five cobbles from a basal transgressive lag deposit sealing a marine terrace referred to as the Last Interglacial (Marine Isotopic Stage 5e). We applied a consistent and highly selective 3-step acceptance criteria on five cobbles and obtained that only one was sufficiently well-bleached prior to burial. The resulting ages of 131 ± 8 ka and 127 ± 8 ka (obtained on 22 analyzed aliquots, n = 22) derived from the post-infrared infrared stimulated signal at 225°C ($pIRIR_{225}$) and the preceding infrared stimulated signal at 50°C ($pIR_{50/225}$), respectively, are consistent with each other as well as with the conventional luminescence age of ~135 ka from the same sequence and with the U/Th age of ~130 ka obtained from coral fragments. This work demonstrates that the RSD is a promising method for dating gravel veneer deposits overlaying marine terraces, enabling new chronologies for similar Quaternary deposits.

1. Introduction

Over fifty percent of the modern worldwide coasts are rocky and characterized by shore platforms (marine terraces) eventually draped by gravelly pocket beaches (Kennedy et al., 2014).

Rocky coasts are characterized by high cliffs and steep beach slopes. The deep seabed prevents gradual waves dissipation making rocky coasts high hydrodynamic environments, where sediments are moved chaotically under a relatively deep water-column and undergo continuous reworking during major storms. In particular, the base of a marine depositional sequence is represented by gravelly or mixed sandy-gravelly deposits (gravelly lags) generated by the erosion of the bedrock during transgression (Zecchin et al., 2019) that can often represent the only depositional record of a Paleo marine terrace. Marine terraces are key landforms for studying paleo-sea level fluctuations and unravelling geodynamic and crustal deformation in tectonic active areas worldwide (e.g., Ferranti et al., 2021; Muhs et al., 2021; Pedoja et al., 2014; Saillard et al., 2017). Traditional dating methods such as radiocarbon and U/Th face significant challenges in dating marine terrace deposits (e.g., Pasquetti et al., 2021 and reference therein) leaving part of the worldwide geomorphic dataset chronologically unconstrained. One of the main research targets is the understanding of the late Quaternary climate changes to forecast the ongoing future. It is therefore of outmost importance to date these surfaces. Over the past 20 years, "abiotic-based" dating methods such as cosmogenic and luminescence have played a significant role in filling this gap in Quaternary geochronology (e.g., Hoffmann et al., 2020; Oakley et al., 2017; Sechi et al., 2020, 2023). The RSD is a novel luminescence method that can date the last exposure to light (burial event) of cobble-sized clasts and/or surface (Simms et al., 2011; Chapot et al., 2012; Souza et al., 2019). This approach has been applied successfully to Holocene gravelly fluvial and beach deposits (Brill et al., 2021; Ishii et al., 2022; Souza

* Corresponding author.
E-mail address: gcossu2@uniss.it (G. Cossu).

https://doi.org/10.1016/j.quageo.2024.101630
Received 14 May 2024; Received in revised form 31 July 2024; Accepted 20 September 2024
Available online 21 September 2024

et al., 2021) but is not yet fully tested on deposits related to Pleistocene marine terraces. Luminescence is based on the ability of certain minerals (mainly quartz and K-feldspar) to act as dosimeters in storing energy from environmental isotopes decay during burial and releasing it under optical stimulations. The phenomenon of complete energy release during sunlight exposure is called bleaching. An assessment of the degree of bleaching (resetting or zeroing) of the luminescence signal before the last burial of the mineral is essential for the reliability of the derived ages. In large clasts such as pebbles and cobbles, sunlight exposure can deplete the latent luminescence signal to depths up to several millimeters beneath the rock surface. This property enables a preliminary evaluation of signal beaching prior to burial, that is not so rapidly achievable in traditional luminescence dating, providing a great advantage for RSD. However, as already documented (e. g. Smith et al., 2023) we obtained scattered ages. To overcome this problem and validate the ages, we have applied a critical workflow adding to the classical evaluation methodology for RSD (sigma-shape and M/N modeling) the principle that: if two signals having different bleaching rates give the same age, partial bleaching can be excluded. The aim of this study is to: i) apply the RSD method to a gravel lag deposit developed at the base of a well-constrained, Late Pleistocene marine terrace sedimentary succession (Marine Isotopic Stage MIS 5e, Sechi et al., 2023 and reference therein) and ii) provide a systematic approach to detect well-bleached cobbles in order to expand the applications of RSD dating to new gravelly marine sequences.

2. Geological setting and sampling site stratigraphy

The studied area, known as Cala Mosca Bay, is located in southern part of the Sardinia Island (Fig. 1). The island occupies a central position in the western Mediterranean region, mostly formed by a series of back-arc basins opened in response to the Alpine/Appennines subduction zone. The Sardinia with the close Corsica Island form a continental block (C-S) detached from southern Europe since the Oligocene. The block is nowadays separating the Algero-Provençal (APB) from the Thyrrenian back-arc basins (Fig. 1) (Doglioni et al., 1998). In Sardinia, this intense Tertiary/Quaternary tectonic activity led to the formation of a series of basins the main of which is NW-SE-oriented Campidano Graben (Casula et al., 2001) (Fig. 1). These are filled by repetitive marine and continental sequences interbedded by volcanoclastic deposits (e.g., Andreucci et al., 2017; Pascucci et al., 2018; Telesca et al., 2020). Sardinia has been considered a quasi-stable block since Late Pleistocene, but new evidence of significant localized vertical movements displacing middle-Pleistocene marine deposits has recently emerged (Casini et al., 2020; Cocco et al., 2019; Sechi et al., 2023).

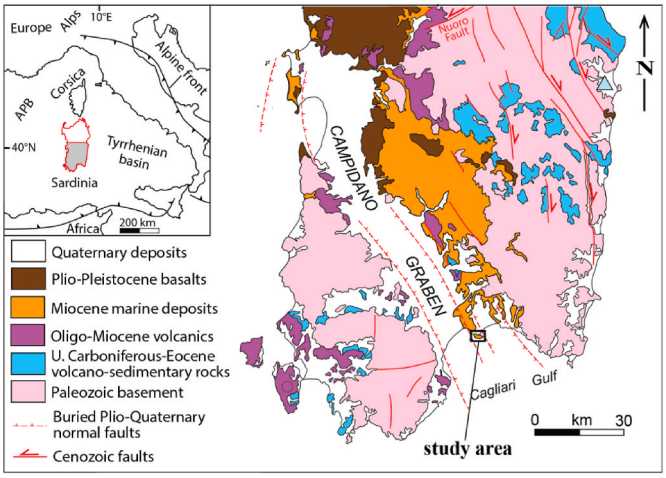

Fig. 1. Overview of the study area and Sardinia main geologic features. The black square indicates the location of the study area of Cala Mosca. The sampling site is located at 39°11′7″ N, 9°8′59″ E (WGS84).

The Late Pleistocene marine succession cropping out at Cala Mosca lies on a terrace carved into the Miocene substrate (Fig. 2). The marine Pleistocene succession cropping out along the area has been studied since the beginning of the century and it is attributed to the last interglacial (MIS5e, 135–119 ka) based on U-series dating of fossil coral finds (Barca et al., 2005 and reference therein).

It is characterized by two unconformably superimposed marine units, U3a and U3b (Fig. 2a). The lower unit (U3a) is made of a basal cobbly transgressive lag (*sensu* Zecchin et al., 2019) passing upward to 3 m-thick regressive mixed sandy gravelly beach face deposits (Fig. 2b). The U3b is characterized by marine sand and gravel deposit related to a second transgression (Fig. 2a). Recent standard luminescence dating referred U3a to MIS 5e (137 ± 7 ka, 134 ± 7 ka) and U3b to MIS 5c (92 ± 6 ka) (Sechi et al., 2023) confirming the previous U/Th-ages made on fossil coral finds (average 130 ka; Barca et al., 2005 and reference therein).

3. Methods

3.1. Sample preparation and luminescence measurements

A preliminary field survey was conducted to select the most suitable cobble samples for OSL RSD dating. Presently the marine section of Cala Mosca forms the sea cliff carved by the wave, with the typical boulder lag at the base due to the partial collapse of the outcrop (Fig. 2a and b). Although collapsing of the cliff makes the outcrops and stratigraphic section visible and accessible, this exposes part of the target deposits to the sunlight. Sampling was limited by the accessibility of the outcrops and by the limited distribution of well-buried suitable cobbles. Furthermore, Cala Mosca is a site of great natural interest to the local community and sampling was conducted to preserve the integrity of the outcrop as much as possible.

The cobbles originate from the erosion of the Miocene sandstone, part of the siliciclastic marine succession called Arenarie di Pirri Formation, cropping out as pre-Quaternary substrate around Cala Mosca Bay (Fig. 2a and b). Thin section analysis shows that the substrate consists of well-sorted, medium-grained siliciclastic sandstone with lithic fragments, abundant amounts of sub-rounded quartz, K-rich feldspar grains and meniscus carbonate cement (see Fig. 2c). Cobbles made of Arenarie di Pirri Formation sandstones from basal transgressive lag of Unit U3a were deemed as optimal target for our study. Five cobbles were chosen based on criteria such as size (~20 cm Ø), lithology type (sandstone), shape (roundedness was interpreted as hint of reworking) and minimum exposed surface (Fig. 2b). The cobbles (CLMr1, CLMr2, CMr3, CLMr4 and CLMr5) were collected at night under subdued red light and the portion of the exposed surface was marked with black ink. The sandy matrix surrounding each cobble was also collected for external environmental dose rate determination.

Cobbles were processed at the Nordic Laboratory of Luminescence Dating, DTU Risø campus and at the Luminescence Dating Laboratory of the University of Sassari under subdued amber light (Sohbati et al., 2017). The surface was drilled using a water-cooled diamond-tipped core drill to obtain ~50 mm long and 20 mm in diameter cores. At least three cores were drilled from each cobble, and then cut at intervals of ~1 mm using a 0.33 mm-thick wafer diamond blade. At least 10 slices were cut from each core from the surface to reach a depth of over 1 cm inside the cobble. Whenever possible, the first 1 mm slices were abraded with a stainless-steel rasp to obtain material from 0.5 mm in depth. It was only possible to perform this measure in samples CLMr1 and CLMr2. It aims to increase the resolution at the surface and better define if a bleaching front plateau (at least two consecutive points with similar L_n/T_n) is present. Each slice was split into aliquots, consisting of sub-slices (or of portion of unsieved powder in the case of material from 0.5 mm) and placed on stainless steel cups, without any chemical treatment. Measurement of aliquots was performed by two Risø

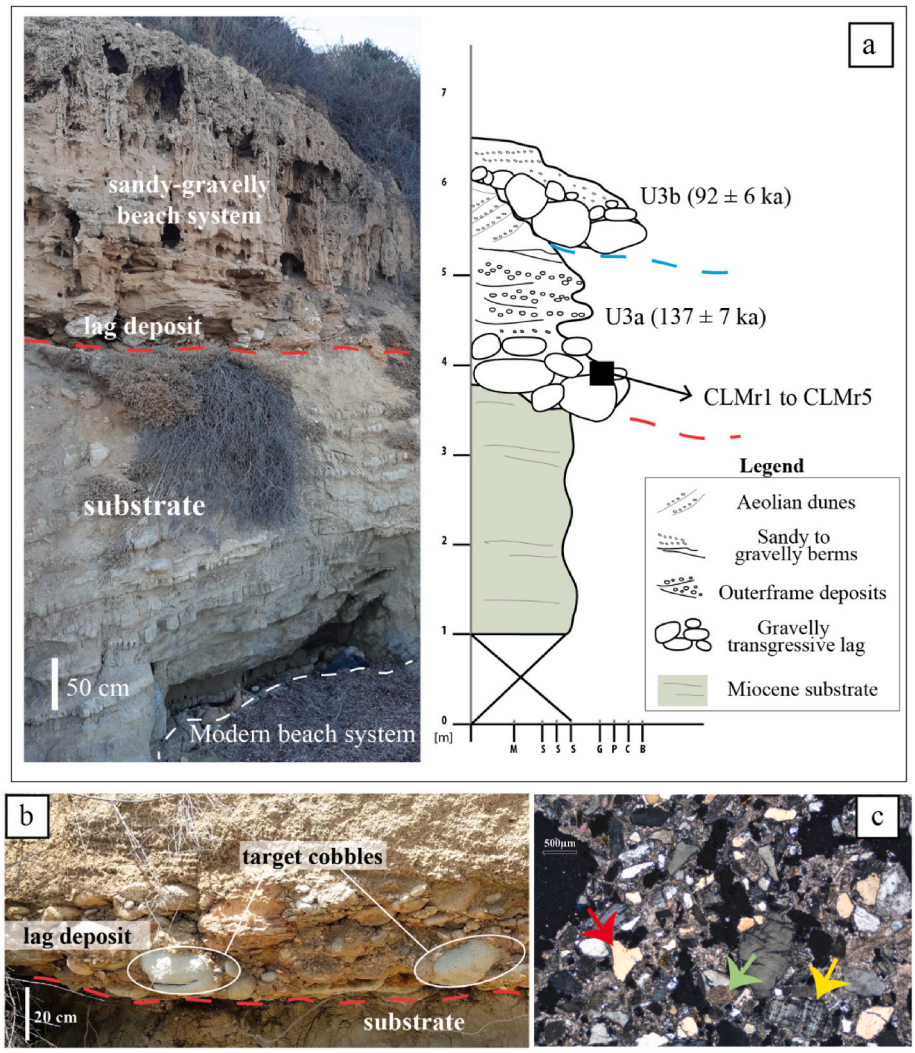

Fig. 2. The late Pleistocene marine deposits cropping out at Cala Mosca bay. a) Field details and stratigraphic Log. The red dashed line represents the erosive surface cutting the substratum at about 3.5 above current sea level. Above Miocene sandstones the transgressive lag deposit lays unconformable, followed by trough cross bedded sandstone (shoreface deposit), passing into low angle bedding (foreshore) and to a well-sorted sandstone with widespread vertical bioturbation (aeolian dune). Reported ages are from Sechi et al. (2023) b) Field details of the transgressive gravelly lag deposits and the rounded sandstone cobbles target of this study. c) Cross-polarized light microscope (XPL) photo of thin section of the sample composed mainly of quartz (red arrow), k-feldspars (yellow arrow) and lithic fragments (white arrow).

TL/OSL-DA-20 readers equipped with $^{90}Sr/^{90}Y$ calibrated beta irradiation sources (0.1216 ± 0.0013 Gy/s and 0.1933 ± 0.002 Gy/s, respectively). Being slices polymineral, to avoid signal contamination they have been analyzed using the Infra-Red stimulation (Souza et al., 2019, 2021). In particular, the two-steps post-Infra-Red (pIRIR) protocols have been adopted to obtain two simultaneously signals; one from the first low temperature stimulation (IR) and one from the second more stable high temperature stimulation (pIRIR). We have measured our samples using $pIRIR_{290}$ and $pIRIR_{225}$ protocols from K-rich feldspar, along with corresponding first IR signals at 50 °C (henceforth named $pIR_{50/290}$ and $pIR_{50/225}$, respectively) (Table 1) (Buylaert et al., 2009; Thiel et al., 2011). The signals were detected through a combination of Shott-BG-39 and Corning 7–59 glass filters, transmitting in blue-violet wavelength range and were calculated by integrating over the first second of stimulation subtracted by a background integrated over the last 10 s.

The sensitivity-corrected natural signal (L_n/T_n) was measured from each aliquot and plotted against the depth of the aliquot to reconstruct the luminescence-depth profile. Each profile was normalized to the field-saturation plateau represented by the average of four L_n/T_n value obtained at depth and fitted using the model representing the expected depositional history for cobbles of interest. Sohbati et al. (2011) demonstrated that the bleaching of luminescence signal as a function of depth during daylight exposure could be described as follows:

$$L_1(x) = L_0 e^{(-\sigma\varphi_0 te)e^{(-\mu x)}} \quad (1)$$

Where L_0 is the initial signal at saturation (equal to 1 in normalized

Table 1
Protocols.[a] SAR $pIRIR_{290}$ and [b] SAR $pIRIR_{225}$ protocol used for signal analysis and Paleodose estimation. The given Test Dose was about 30 Gy.

Step	Measurement
1 Natural or Regenerative Dose	L_n or Lx (Beta irradiation)
2 Preheat	Heating at 320[a]/250[b] °C for 100 s
3 IR stimulation	IR LEDs at 50 °C for 100 s
4 pIRIR stimulation	IR LEDs stimulation at 290[a]/225[b] °C for 100 s
5 Test Dose	T_n or T_x (Beta irradiation)
6 Cutheat	Heating at 320 [a]/250[b] °C for 100 s
7 IR stimulation	IR LEDs at 50 °C for 100 s
8 pIRIR stimulation	IR LEDs stimulation at 290[a]/225[b] °C for 100 s
9 Cleanout	IR LEDs at 325[a]/290 °C for 100 s

profiles), x (mm) is the depth from surface, t_e is the exposure time (ka), σ (cm^{-1}) is the photoionization cross section, φ_0 is the photon flux (cm^2 s^{-1}) at the surface of the rock and μ (mm^{-1}) is coefficient of light attenuation with depth.

The bleached signal will regrow during a subsequent burial event resulting in a profile described by the equation proposed by Freiesleben et al. (2015):

$$L_2(x) = (L_1(x) - 1)e^{(-F(x)tb+1)} \quad (2)$$

Where t_b is the burial time (ka), *F(x)* represents the trap-filling rate and is calculated as the ratio between the depth-dependent dose rate (Gy ka^{-1}) and the characteristic dose (D_0).

In this study, profiles were fitted assuming a single bleaching event followed by a single burial event (i.e. equation (2)).

The light attenuation coefficients μ and photoionization cross-section σ are two paramount parameters for fitting luminescence depth profiles with an unknown time of first exposure. The bleaching ability of the lithology was assessed by cutting in half two representative cobbles (CLMr1 and CLMr2) to obtain inner surfaces, with luminescence signal in field saturation, that were exposed to sunlight for 30 days ($0.08*10^{-3}$ ka) during Sardinian Summer. Obtained bleaching L_n/T_n profiles were measured up to 8 mm in depth and fitted with equation (1), in order to obtain bleaching physical parameters (μ, $\sigma\varphi_0$) characteristic for the analyzed lithotype and then to forecast the L_n/T_n profile shape just before burial (Sohbati et al., 2011).

Using the above parameters and equations of single exposure/burial events, the measured buried profile (thereafter named N, fitting with equation (2)) and the predicted profile at burial time (thereafter named M, equation (1)) can be used to define if the signal at surface has been properly reset. The ratio M/N (%) describes the variation of the residual signal with depth before the burial event. As proposed firstly by al Khasawneh et al. (2019), under the 3% of M/N a surface can be defined well bleached. Later, Souza et al. (2021) proposed to elevate the M/N threshold at 5%, this value is used in this work.

On cores that resulted to be well bleached at the time of burial, the equivalent dose (D_e) at the depth of interest (1 mm) was obtained using at least six aliquots for each core and plotting the natural sensitivity corrected signal (L_n/T_n) on the regenerated dose-response curve (DRC) fitted using a single exponential function. Criteria of recuperation (below 5% of natural signal) and recycling values (0.9–1.1) were used to reject unreliable aliquot.

Anomalous fading was calculated with the Natural-to-Laboratory-Saturation (NLS) ratio proposed by Rades et al. (2018), taking advantage from the fact that the sandstone source of the cobbles is Miocene in age, thus the signal at the innermost part of the cobble reached natural saturation. Following these authors, fading can be estimated by the ratio of natural field saturation to administered laboratory saturation level $(L_n/T_n)/(L_{sat}/T_{sat})$, named NLS ratio, which gives a direct measure of the upper limit and the fading effect on the natural signal. The NLS ratio can be used directly to correct luminescence signal loss during burial. To do this, an innermost slice (~5 cm deep) was used and the natural field saturation (L_n/T_n) was determined on three aliquots, whereas the laboratory saturation values (L_{sat}/T_{sat}) was evaluated on three different aliquots irradiated in laboratory with a dose of ~3000 Gy given on top of the natural.

3.2. Dose rate calculation and modeling

The primary step is to estimate the bulk, infinite matrix, alpha, beta and gamma dose rates of the cobble and the surrounding material (matrix) (Sohbati et al., 2015). Portions of cobbles and matrix (~300 g each) were powered and sealed with wax into a fix-geometric shape to retain radon emission, and the natural activity of ^{238}U, ^{232}Th and ^{40}K radionuclides were estimated using HpGe Gamma spectrometry following Murray et al. (2018, 1987). For dosimetry, the combined dose rates of the K-rich feldspar crystals (internal dose rate), the dose rate of cobble itself and the surrounding sediments (matrix), as well as cosmic radiation (cosmic dose rate) are considered for dating. The average 275 μm grain size of the material constituting cobbles was estimated by soaking a portion of each cobble (~250 g) in a 40% HCl bath and measuring the grain size distribution of loose material and used for grain size correction. Radionuclide activities were converted to cobble and matrix dry total dose rates using the conversion factor of Guérin et al. (2011) and Cresswell et al. (2018) (Table 2). We add a beta dose rate of 1.07 ± 0.04 Gy/ka as K-rich feldspar internal self-dose assuming a concentration of 12.5 ± 0.5% for ^{40}K and 400 ± 100 ppm for ^{87}Rb (Huntley and Baril, 1997, Readhead, 2002). Grain size attenuation was calculated based on Guérin et al. (2011) and on Brennan et al. (1991) for beta and alpha dose rates, respectively.

The variation of the β dose rate with depth was modeled following Souza et al. (2019) based on the equation:

$$D\beta(tot) = 0.5D\beta(cobble) + 0.5D\beta(cobble)*\left(1 - e^{(-bx)}\right) + 0.5D\beta(matrix)*e^{(-bx)} \quad (3)$$

Where 0.5 correspond to the fractional contribution of external and internal β dose rate at the interface, Dβ (cobble) is the infinite-matrix beta dose rate of the rock (Gy ka^{-1}), Dβ (matrix) is the water content corrected infinite matrix beta dose rate of the matrix associated to each cobble (Gy ka^{-1}), b is the beta linear attenuation coefficient in the cobble (mm^{-1}), modified for the rock density (~2.4 g/cm^3) and x (mm) is the depth of interest from the surface. The variation of the matrix and cobble beta dose rate mutual contribution is presented in Fig. S1. The same equation is used to calculate the gamma effective dose rate Dγ (tot), with further correction of the fractional γ-contribution at the surface and γ attenuation coefficient for each cobble diameter following Riedesel and Autzen (2020). Finally, the cosmic radiation contribution was added (Prescott and Hutton, 1994) together with the alpha dose rate due to in ternal ^{238}U and ^{232}Th (0.1 ± 0.05 Gy/ka) (Smedley and Pearce, 2016) were added. The total dose rate was then corrected for moisture content of the matrix (Aitken, 1985) (Table 2). The measured ^{238}U and ^{232}Th activity distribution are consistent for all cobbles, whereas the ^{40}K shows slightly distribution variability (Table 2). To account for the ^{40}K lithological variability, the averaged potassium internal dose of all cobbles is considered more representative of source material and used for dose rate modeling.

4. Results

4.1. Luminescence proprieties

In order to verify the presence of suitable luminescence properties in the collected cobbles preliminary tests such as signal sensitivity, dose recovery and the shape of the luminescence-depth profiles were investigated on sample CLMr2. Luminescence signal sensitivity was tested from the natural sensitivity-corrected signals (L_n) in response to a test dose (T_n) for $pIRIR_{225}$ and $pIRIR_{290}$ protocols and $pIR_{50/225}$ and $pIR_{50/290}$ signals showing bright shine-down curves (Fig. 3a). Both $pIRIR_{225}$ and $pIRIR_{290}$ luminescence-depth profiles have a sigmoidal shape (S-shape) with a significant increase of L_n/T_n from the surface toward a continuous L_n/T_n ratio in field saturation with depth (Fig. 3b). Similar profile shape has been observed for the $pIR_{50/225}$ and $pIR_{50/290}$.

The reproducibility and reliability of the measurement protocols were assessed with a dose recovery test. Two slices of the innermost part of the cobbles with signal in field saturation were bleached for ten days under a Hönle SOL 2 solar simulator. The amount of unbleachable residual signals is 25 ± 1.7 Gy ($pIRIR_{290}$), 5.5 ± 1.4 Gy ($pIRIR_{225}$), 4.76 ± 0.36 Gy ($pIR_{50/290}$) and 0.98 ± 0.18 Gy ($pIR_{50/225}$), respectively. A dose close to the natural (about 250 Gy) was administered to bleached slices, and the recovered dose was measured. The calculated dose recovery ratios (recovered dose/given dose) after residual subtraction

Table 2
Dose Rate results. Summary of the main radionuclides activities, the calculated dry infinite matrix beta and gamma dose rate for the external (matrix) and internal (cobble) contribution evaluation. Alpha values* presented for the cobbles are attenuated for the average grain size of 275 μm. Parameters that affect dose rate attenuation, such as matrix water content (%) and cobble density (g/cm^3) and diameter (cm) are also presented.

Sample	Sampling depth (cm)	Water content (%)	^{238}U (Bqkg^{-1})	^{226}Ra (Bqkg^{-1})	^{232}Th (Bqkg^{-1})	^{40}K (Bqkg^{-1})	β dose rate (Gyka^{-1})	γ dose rate (Gyka^{-1})	α dose rate* (Gyka^{-1})	Density (g cm^{-3})	Diameter (cm)
Matrix											
M1	–	4.09	9.4 ± 1.3	8.6 ± 0.2	5.2 ± 0.1	343 ± 4	1.23 ± 0.03	0.48 ± 0.01	–	–	–
M2	–	4.1	15.2 ± 4.4	8 ± 0.3	5.2 ± 0.3	504 ± 9	1.43 ± 0.01	0.53 ± 0.01	–	–	–
M3	–	3.4	15.9 ± 5.1	12.9 ± 0.3	23.08 ± 0.47	899 ± 14	2.57 ± 0.04	1.09 ± 0.04	–	–	–
M4	–	1.3	16.9 ± 3.5	12.9 ± 0.3	3.4 ± 0.2	75 ± 4	0.37 ± 0.002	0.21 ± 0.006	–	–	–
M5	–	2.3	10.8 ± 1.1	10.7 ± 0.17	2.7 ± 0.1	32 ± 2	0.21 ± 0.01	0.14 ± 0.002	–	–	–
Cobbles											
CLMr1	100	–	14.33 ± 33	6.5 ± 25	10.5 ± 0.6	646 ± 14	1.8 ± 0.18	0.69 ± 0.21	0.013 ± 0.02	2.4	17
CLMr2	200	–	8.5 ± 8.9	5.6 ± 0.7	10.7 ± 0.7	641 ± 17	1.76 ± 0.02	0.66 ± 0.04	0.01 ± 0.05	2.4	20
CLMr3	100	–	8.1 ± 3.5	8.5 ± 4.3	10.8 ± 0.3	518 ± 11	1.46 ± 0.02	0.59 ± 0.04	0.001 ± 0.005	2.4	18
CLMr4	100	–	8.1 ± 3.9	8.4 ± 3.5	14.3 ± 0.3	545 ± 9	1.6 ± 0.02	0.65 ± 0.03	0.15 ± 0.05	2.4	17
CLMr5	150	–	10.8 ± 3.8	5.1 ± 4.6	13.1 ± 0.4	552 ± 11	1.6 ± 0.004	0.63 ± 0.01	0.016 ± 0.005	2.4	18
CLMr -AVG		–	**9.99 ± 1.2**	**6.8 ± 0.7**	**11.9 ± 0.7**	**580 ± 26**	**1.64 ± 0.04**	0.66 ± 0.01	0.015 ± 0.01		

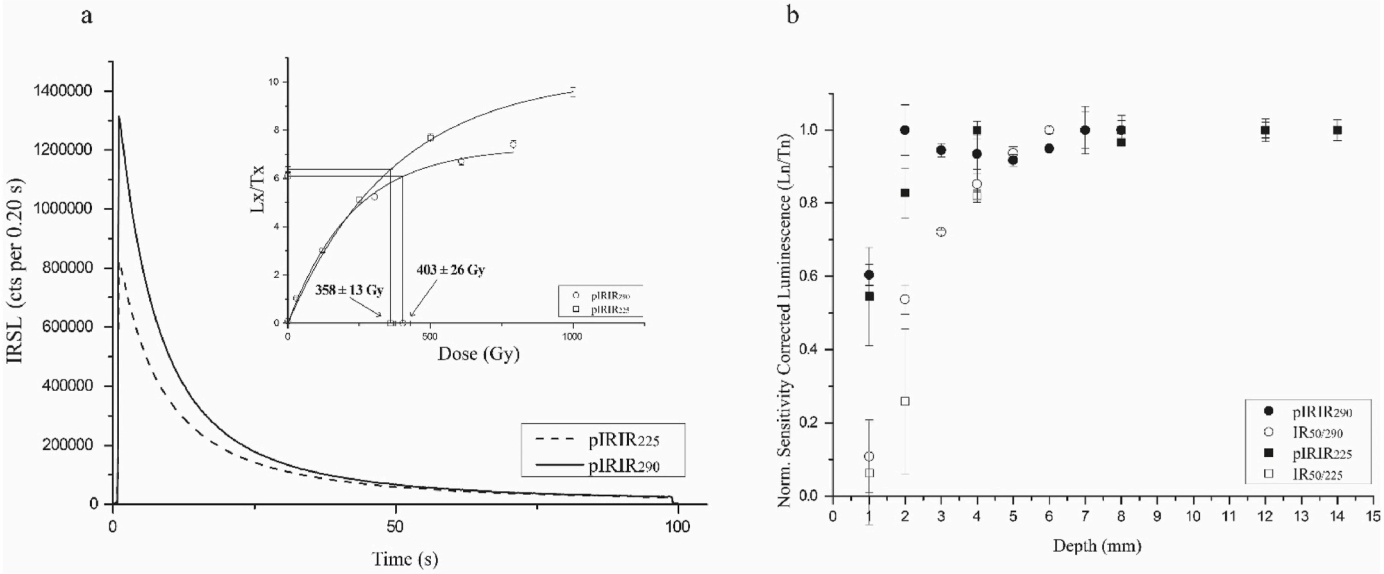

Fig. 3. Luminescence characteristics of the analyzed signals. a) Variation with depth of the natural sensitivity corrected (L_n/T_n) pIRIR$_{290}$ and pIRIR$_{225}$ signals (circles and squares, respectively). Empty symbols represent relative pIR$_{50/290}$ and pIR$_{50/225}$. The natural signal was analyzed until 14 mm in depth, each point representing the average of three aliquots with relative standard errors. b) An example from sample CLMr2 of the Decay curves and Dose Response Curves (DRC) of pIRIR$_{290}$ and pIRIR$_{225}$ signals.

significantly overestimated the given dose for pIRIR$_{290}$ (1.46 ± 0.11) while the pIR$_{50/290}$ resulted slightly underestimated (0.87 ± 0.01). In contrast, dose recovery ratio provided acceptable values for pIRIR$_{225}$ (0.91 ± 0.02) and pIR$_{50/225}$ (1.01 ± 0.03). Despite pIRIR$_{290}$ protocol shows a good S-shape curve due to the unacceptable dose recovery test it was dismissed and further tests were conducted on pIRIR$_{225}$ signals.

The equivalent doses (D_e) for pIRIR$_{225}$ protocol at the cobble surface are not in saturation (Fig. 3b), average recycling values are 0.99 ± 0.012 (pIRIR$_{225}$) and 0.99 ± 0.01 (pIR$_{50/225}$) and recuperation values are 0.91 ± 0.07 (pIRIR$_{225}$) and 2.40 ± 0.57 (pIR$_{50/225}$) (Fig. S2). Given the satisfactory performance of pIRIR$_{225}$ and pIR$_{50/225}$ along with the acceptable recycling ratio (close to the unity) and recuperation (less than 5% of natural) this is the chosen signal for dating Cala Mosca unit U3a cobbles.

Finally, the loss of natural signal due to anomalous fading has been investigated for both pIRIR$_{225}$ and pIR$_{50/225}$ signals calculating the NLS ratio. The NLS ratios have been calculated on samples CLMr1 and CLMr2, resulting in 0.78 (CLMr1) and 0.76 (CLMr2) for the pIRIR$_{225}$ and 0.58 (CLMr1) and 0.5 (CLMr2) for pIR$_{50/225}$. Considering the homogeneity on the source of the K-feldspars, the average value was assumed to be consistent and used for NLS fading correction of the other samples.

4.2. Luminescence-depth profiles

The luminescence-depth profiles using pIRIR$_{225}$ and pIR$_{50/225}$ protocols were measured for at least three cores collected on one side of

each cobble (five in total) and fitted using Equation (2). The obtained parameters reported in Table 3. Selection and rejection of single cores have been based on the process flowchart (Fig. S3) and the result are summarized in Table 4 for both $pIRIR_{225}$ and $pIR_{50/225}$. Profiles shape for total analyzed cores is presented in Fig. 4.

The luminescence-depth profiles of $pIRIR_{225}$ signal for CLMr1 and CLMr2 (Fig. 4) shows a sigmoidal shape for all the three analyzed cores with an increasing L_n/T_n ratio toward field saturation after 2 mm in depth.

For cobble CLMr3, only two cores C2T and C3T show a sigmoidal shape profile reaching complete field saturation reached at ~3 mm (C2T) and ~4 mm (C3T). Core C1T (CLMr3), instead, show a signal in continuous field saturation from the surface, therefore it was considered unreliable and rejected.

For cobble CLMr4, only C1T and C2T cores have sigmoidal shapes, and the complete field saturation reached at 2 mm depth. Core C3T (CLMr4) show a signal in continuous field saturation from the surface, therefore it was rejected.

All three cores of cobble CLMr5 show a poorly developed sigmoidal shape profiles with a potential bleaching front at 1 mm depth and a field saturation at 2 mm.

The same process flow has been applied to the $pIR_{50/225}$ luminescence depth profiles (Table 4). The analysis of $pIR_{50/225}$ signal (Fig. S5) highlight that three cores of cobble CLMr1, CLMr2r and CLMr4 have well-defined sigmoidal luminescence depth profiles while CLMr3 and CLMr5 have $pIR_{50/225}$ luminescence depth profiles with very poorly developed sigmoidal shapes (Fig. S5).

4.3. Bleaching determination

A potential bleaching front at 1 mm of depth has been observed in at least two cores for all cobbles and has been considered the target depth to be investigated. This is confirmed by bleaching profiles resulting from one month of daylight exposure (Fig. 5) where the signal resulted zeroed up to of 1 mm ($pIRIR_{225}$) or 3 mm ($pIR_{50/225}$) in depth for sample CLMr1 and up to 0.5 mm ($pIRIR_{225}$) or 1 mm ($pIR_{50/225}$) in depth for sample CLMr2. To verify whether cobbles experienced enough light exposure of the surface before burial, analyzed profiles were fitted and the predicted profile-shape at the time of burial (Sohbati et al., 2015) was modeled (Fig. 6a, S4, S5). Thus, M/N ratio for the target depth of 1 mm for each chosen core was calculated, and according to previous works, we set as rejection criteria a residual equal to 5% of the natural signal. The M/N ratio is reported in Fig. 6b, S4 and S5, where the horizontal dotted line represents the threshold (5 %). Regarding $pIRIR_{225}$ signal (Fig. 6b), for CLMr1, the M/N ratio is lower than 5% at depth 2.2 (C1T), 0.7 (C2T) and 2 mm (C3T) with an average value of 1.6 mm (Fig. 6b). For CLMr2, the limit of 5% is reached at a depth of 1.3 (C1T), 0.8 (C2T) and 0.7 (C3T), with an average of 0.8 mm (Fig. 6b). For Cobble CLMr3 (Fig. S4), core C1T profiles cannot be fitted, while core C2T have an M/N ratio <5% at 1.4 and C3T is rejected with a ratio higher than 5% at the target depth. For CLMr4 only core C2T has the M/N ratio lower than 5% at 1 mm, while profiles for cores C1T and C3T cannot be fitted and thus rejected (Fig. S4). For cobble CLMr5, all the measured cores failed the fitting procedure.

Same approach was applied to $pIR_{50/225}$ signal (Fig. S5). The M/N ratio for both CLMr1 and CLMr2 reached the threshold limit at about 2.2 mm of depth in average. For CLMr4 the M/N ratio is variable among cores with <5% at 1.6 mm (C1T), 0.8 mm (C2T) 2.2 mm (C3T), reaching the limit in average at 1.2 mm. Cobbles CLMr3and CLM5r failed profile fitting and thus are considered unreliable. It is worth noting that, for the two analyzed signals, the fitting produced with equation (2) does not always accurately describe the trend of the analyzed points (Fig. 6, S4, S5). T his certainly has an impact on the M/N results.

Table 3
Fitting parameters. Average values of obtained fitting parameters, based on of Freiesleben et al. (2015).

Sample	pIR_{225} μ (mm^{-1})	$pIR_{50/225}$ μ (mm^{-1})	pIR_{225} teσφ0	$pIR_{50/225}$ teσφ0
CLMr1	0.75 ± 0.06	0.86 ± 0.03	13 ± 4	27 ± 3
CLMr2	1.49 ± 0.29	0.86 ± 0.03	15.8 ± 3	7.7 ± 1.7

Table 4
Rejection criteria results. Results for each step of rejection criteria applied on CLMr samples. For each core (C1T, C2T, C3T) the profile shape (**SP, rejection step a**) was evaluated, and cores were accepted (**A**) or rejected (**R**) based on the presence of a sigmoidal shape profile. Passed this step, cores were fitted with equations proposed by Freiesleben et al. (2015) and cores with an M/N ratio beyond 10% at 1 mm (**M/N, rejection step b**) were rejected and not further analyzed. Furthermore, the cores that failed fitting procedure (**NF**) were also rejected at this step. Those steps were applied both on $pIRIR_{225}$ and for $pIR_{50/225}$ signals. For all the cores that passed the first two step the fading-corrected age (**Age*, rejection step c**) was calculated. Finally, the reliability is evaluated based on age homogeneity between cores belonging the same cobble and possibly among ages obtained with two different signals.

Rejection steps →		$pIRIR_{225}$		$pIR_{50/225}$		$pIRIR_{225}$	$pIR_{50/225}$
		a	b	a	b	c	c
Cobble	Core	SP	M/N at 1 mm	SP	M/N at 1 mm	Age* (ka)	Age* (ka)
CLMr1	**C1T**	A	<5%	A	<5%	**133 ± 8**	**124 ± 8**
	C2T	A	5<%<10	A	<5%	**129 ± 8**	**134 ± 8**
	C3T	A	<5%	A	<5%	**129 ± 8**	**124 ± 8**
CLMr2	**C1T**	A	<5%	A	<5%	121 ± 7	12 ± 0.7
	C2T	A	5<%<10	A	R	179 ± 10	–
	C3T	A	R	A	R	–	–
CLMr3	**C1T**	R	NF	R	–	–	–
	C2T	A	<5%	A	NF	14 ± 3	–
	C3T	A	R	A	R	–	–
CLMr4	**C1T**	A	NF	A	<5%	–	167 ± 14
	C2T	A	<5%	A	5<%<10	180 ± 14	150 ± 12
	C3T	R	NF	A	<5%	–	52 ± 8
CLMr5	**C1T**	A	NF	A	NF	–	–
	C2T	A	NF	A	NF	–	–
	C3T	A	NF	A	NF	–	–

5. Discussion

Five clasts were collected from the cobbly transgressive lag at the base of the Middle-Pleistocene marine succession, draping the wave-cut platform of the Cala Mosca marine terrace.

Obtained burial ages resulted scattered underestimating and overestimating the expected age of ~130 ka. In order to discriminate which ages must be deemed valid, a three-steps rejection method (a, b, c) is used to validate the results (Fig. S3):

a) Visual evaluation of the observed luminescence depth profile. A sigmoidal shape is a good indicator of surface bleaching before burial (Fig. S3a).
b) Profile modeling and M/N ratio. This parameter can predict the variation of the residual signal with depth. In the literature, the M/N threshold considered acceptable is 5%, however, since the values we obtained are very fluctuating we arbitrarily decided to extend the analysis to single profiles whose ratio at first millimeter is <10 % (Table 4) to make the rejection parameter less firm (Fig. 3b)
c) Comparison between different signals with different sensitivities to light. When sediments have undergone sufficient light exposure and the entire luminescence system is fully bleached prior to deposition,

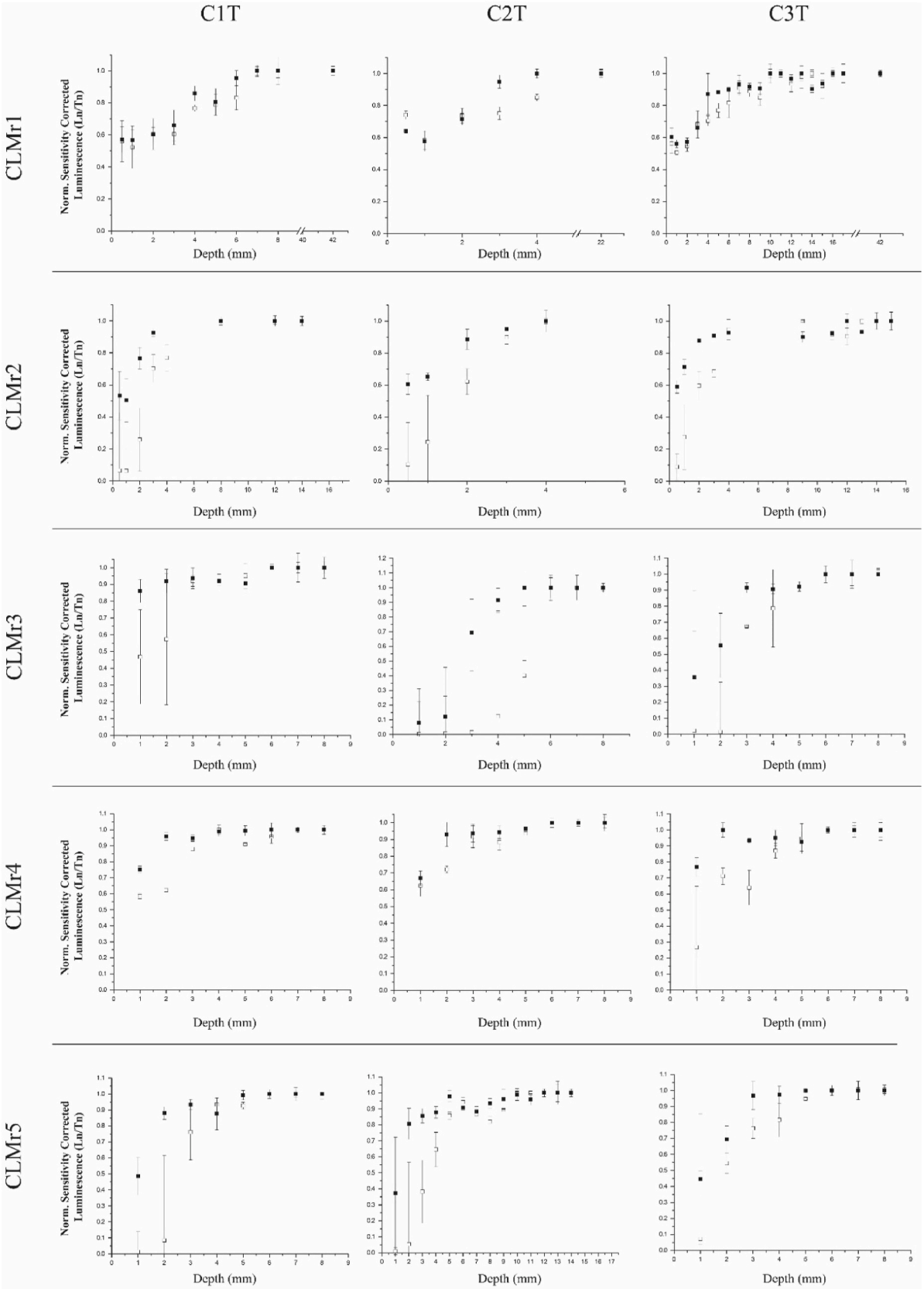

Fig. 4. Natural (L_n/T_n) luminescence-depth profile shapes observed in Cala Mosca samples, normalized to the saturation level. Profile shapes are presented in detail for each core (C1T, C2T, C3T) analyzed in the five samples. Black full and empty squares represent the variation of $pIRIR_{225}$ and $pIR_{50/225}$ signal, respectively, each point representing the average of three aliquots with relative standard errors. The natural signal was analyzed continuously at 1 mm intervals up to 16 mm in depth, and when possible, a deep "back-slice" was analyzed from the base of the cores.

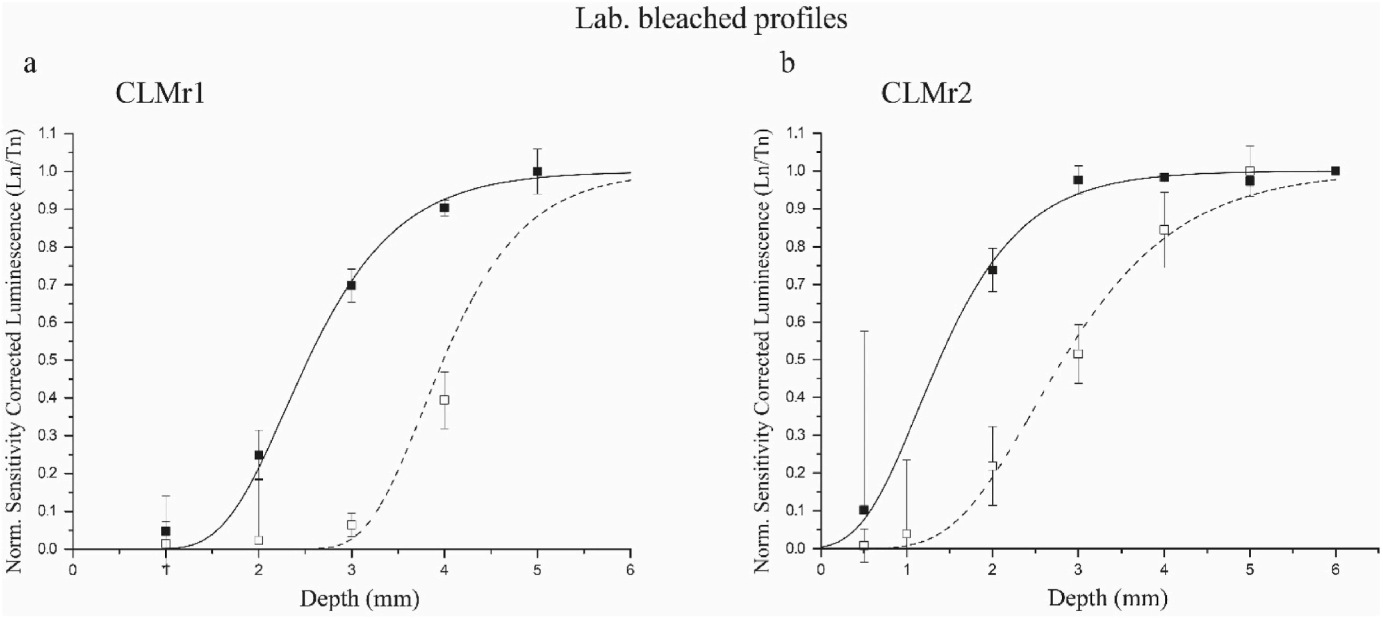

Fig. 5. Luminescence variation with depth of the residual signal after 1 month of daylight exposure of the inner (saturated) surface. Resulting profiles were fitted with Equation 1. a) In sample CLMr1 residual signals are zeroed up to a depth of 1 mm for $pIRIR_{225}$ (full squares) and 3 mm for $pIR_{50/225}$ (empty squares). b) In sample CLMr2 $pIRIR_{225}$ signal (full squares) resulted bleached at about 0.5 mm whereas the $pIR_{50/225}$ (empty squares) is totally zeroed at 1 mm in depth.

different signals should yield comparable burial ages (Murray et al., 2012) (Fig. S3c). Specifically, the IR_{50} signal is known to bleach more rapidly in sunlight compared to pIRIR signals stimulated at elevated temperatures ($pIRIR_{225}$).

For all the cores that completely pass the rejection criteria and are considered sufficiently bleached before burial at the target depth of 1 mm, the equivalent doses are calculated and the obtained fading-corrected ages are given in Table 4. At the end of the process the calculated ages have been compared with previously performed independent ages.

5.1. Sample acceptance and ages

The five investigated cobbles show bright and reproducible luminescence K-feldspar IR-response signals ($pIRIR_{225}$ and $pIR_{50/225}$) and almost all measured cores (13 over 15), had a bleaching profile with decreasing luminescence signals ($pIRIR_{225}$ and $pIR_{50/225}$) from field saturation to lower values at the surface (Table 4). However, it does not testify that a complete and homogenous signal resetting occurred before burial at the target depth (1 mm) (Sohbati et al., 2011). In our case, the analyzed depth profiles revealed a rather shallow front plateau, often not extending the first millimeter. Consequently, doubts arise regarding the completeness of signal resetting to sufficiently low values prior to burial. Bleaching experiments on the lithology of interest demonstrated that after 30 days of direct and undisturbed exposure to sunlight, the signals can be depleted from field saturation to zero at the target depth.

We applied the proposed M/N ratio criteria. In our case this parameter shows a significant variability among samples and within cores of the same cobble. Furthermore, occasionally the M/N value was >5% at a depth slightly shallower than the target depth (Table 4). Therefore, to avoid rejection of potentially reliable data, cores exceeding the 5% but still below the 10% at 1 mm are considered conditionally accepted for the step b) (Table 4). Among the five cobbles, CLMr1 met the 5% M/N criteria for two out of three cores for $pIRIR_{225}$ luminescence-depth profiles, whereas core C2T showed a residual of about 9% at the target depth. However, the average value between the cores results below the 5% of M/N ratio and thus the selected cobble surface is considered reliable. Furthermore, $pIR_{50/225}$ profiles of sample CLMr1 fully meet the M/N criteria (Table 4).

Cobble CLMr2 satisfied the criteria for two cores for $pIRIR_{225}$ and one core for $pIR_{50/225}$. Cobbles CLMr3 and CLMr4 satisfied the criteria solely for one core for $pIRIR_{225}$, whereas for the $pIRIR_{50/225}$ only two cores from CLMr4 were accepted. In contrast, cobble CLMr5 was rejected and deemed unsuitable due to saturated signal at the surface and to difficulty in fitting the profiles (Table 4).

Regarding cobble CLMr1, fading-corrected $pIRIR_{225}$ and $pIR_{50/225}$ burial ages are consistent for all the cores measured, yielding an average age of around 130 ka (Table 4, Table 5). Burial-ages are in agreement with independent ages obtained by Luminescence standard ages performed on the sediment (Sechi et al., 2023) and with U-series on coral finds (about 130 ka in average, Barca et al., 2005; Hearty, 1986). Agreement of fading-corrected $pIRIR_{225}$ and $pIR_{50/225}$ ages for sample CLMr1 reinforce the applied rejection criteria and support that the whole surface of the cobble was well bleached before burial with at least at the target depth of 1 mm.

In contrast, for sample CLMr2 although some luminescence-depth profiles for $pIRIR_{225}$ have passed the rejection criteria, the obtained ages are more difficult to interpret because one core strongly overestimate (179 ± 10 ka) the other, instead, slightly underestimate (121 ± 7 ka) the expected age (ca. 130 ka). The $pIR_{50/225}$ burial-ages of the same cobble, instead, are consistently younger than expected, severely underestimating age controls and stratigraphic interpretation. None of the cores from CLMr2 yield ages obtained with the two different signals that are congruent, suggesting a possible heterogeneous resetting of the surface before burial.

Regarding Cobble CLMr4, obtained ages are scattered, and when we were able to obtain two ages from the same core (CLMr4, C2T) these turned out to be different and not overlapping even with the errors (180 ± 14 ka for $pIRIR_{225}$ and 150 ± 12 ka for $pIR_{50/225}$). Then any of the age can be validated.

Two clasts (CLMr3 and CLMr5) have signals mostly continuous from the surface and are thus deemed unreliable for dating as they did not pass the rejection criteria.

Our research suggests that a successful approach lies in measuring the bleaching of gravel lag deposits that seal the shore platform. To ensure reliable ages with reduced cobble rejection, we implemented a comprehensive screening procedure to select well-bleached cobbles,

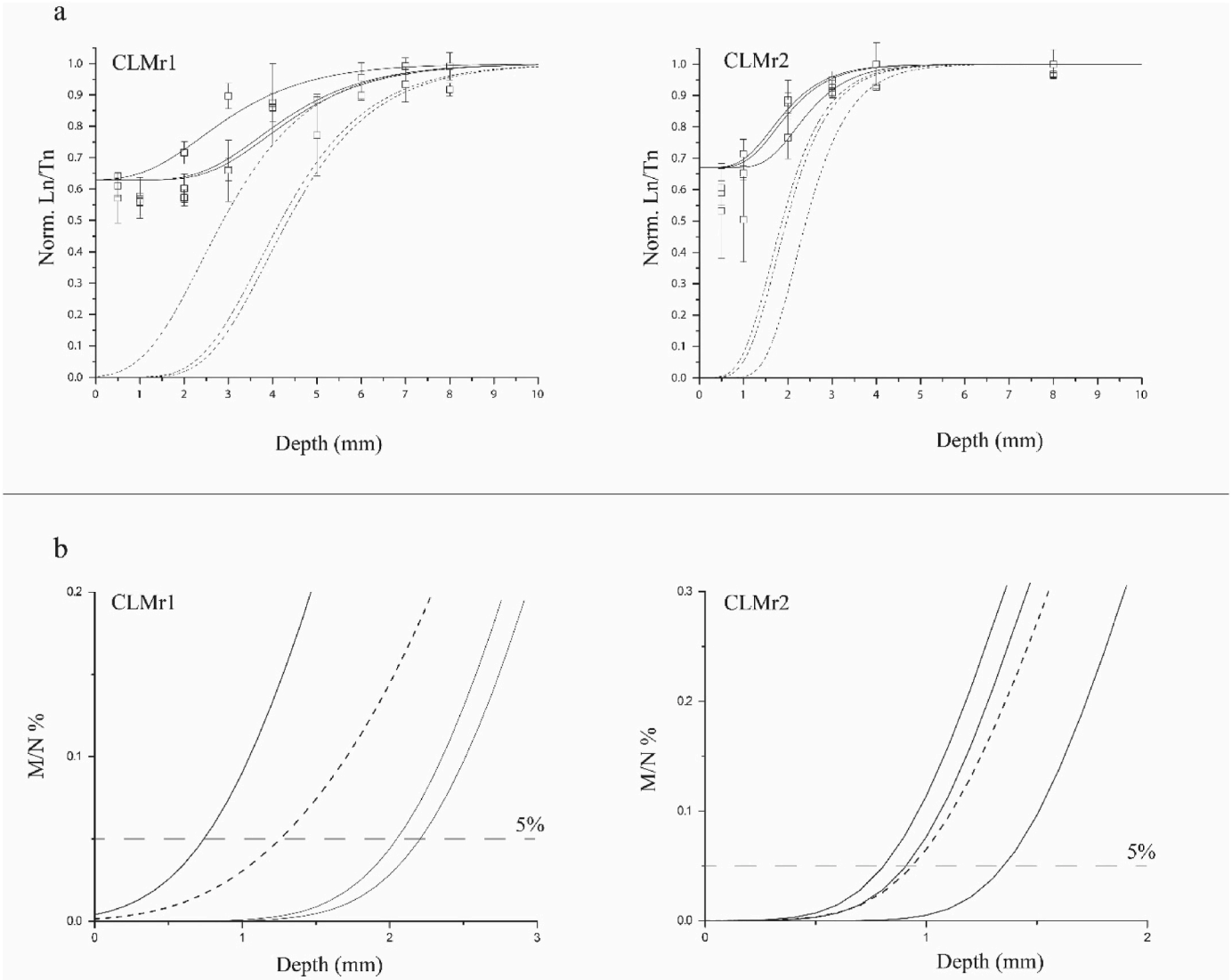

Fig. 6. Results from modeling and M/N variation of $pIRIR_{225}$ signals in two representative samples (CLMr1 and CLMr2). All modeled profiles for the samples analyzed in this study are available in supplementary material section (Figs. S4 and S5 for the $pIRIR_{225}$ and the $pIR_{50/225}$ signals, respectively). a) Results from fitting of natural observed $pIRIR_{225}$ signal variation (N, solid lines) and modeled signal variation before burial (M, dashed lines) of samples. Analyzed points are reported as squares, each point representing the average of three aliquots with relative standard errors. b) M/N ratio (%) variation with depth for each core is shown in solid lines, whereas the average of the sample is represented as a dashed line. Horizontal dotted line represents the threshold (5 %) considered in this study. Cores which M/N profile at 1 mm depth is below 5% are considered accepted for the criteria established from literature (e.g., Souza et al., 2019), whereas cores exceeding the 5% but still below the 10% at 1 mm are considered conditionally accepted in this work.

Table 5
Final ages. Summary of the luminescence results. Sample CLMr1 was considered fully reliable for RSD, and the final age was calculated using aliquots from all analyzed cores. Fading corrected ages were obtained by dividing the uncorrected age by the proper NLS ratio. N is the number of aliquots used for Paleodose determination; Rd is the unbleachable residual.

Sample	N	Signal	De (Gy)	Rd (Gy)	NLS fading ratio	Dose rate at 1 mm depth ($Gyka^{-1}$)	Uncorrected age (ka)	Corrected age (ka)
CLMr1	22	**$pIRIR_{225}$**	325 ± 6	15 ± 1.5	0.78	3.031 ± 0.073	103 ± 7.	**131 ± 8**
CLMr1	22	**$pIR_{50/225}$**	225 ± 6	3 ± 0.2	0.58	3.031 ± 0.073	74 ± 6	**127 ± 8**

encompassing careful sampling and depth-profile determination. While the initial assessment of the presence of a front plateau can serve as a valuable indication of potential surface bleaching and saturation of signal at the surface, it should not be regarded as the sole determining factor. Many clasts become rapidly imbricated and buried in this dynamic environment leading to a heterogeneous degree of bleaching among clasts and within the same cobble surface. Nevertheless, others have time to be exposed to light, even if for a short time sufficiently to undergo not deep complete surface bleaching. The M/N ratio proves to be a valuable parameter in determining the potential bleaching of the cobble surface prior to burial (al Khasawneh et al., 2019). However, w hen the front plateau is underdeveloped or very shallow (less than 2 mm), a threshold of 5% is too restrictive, leading to the rejection of potentially reliable cores. In fact, samples yielding potentially rejected cores (e. g. C2T in CLMr1) but in which average value of M/N is below the threshold and ages obtained from single cores are consistent, should

be considered reliable.

5.2. Environmental implication for RSD

An advantage of rock surface luminescence methods over those applied to sand and silt is that it raises for the first time the possibility of direct measurement of the burial chronology of clast eroded from the terrace and deposited as gravel lag onshore during transgression and the following sea still stand. However, as with other sedimentary environments, confidence in completely resetting of luminescence signal before burial is a paramount element for reliable rock surface dating. Unlike terrestrial chaotic mass transportation (such as debris flow, mega flood and river flood) that experience long period of light and exposure of clast and a rapid transport and burial (Cunningham et al., 2018; Smith et al., 2023), marine gravel lags forms in shallow water from waves abrasion of the substrate with the accumulation of reworked cobble clast-size from the substrate directly upon the shore platform. In such active littoral dynamics, clasts experience continuous reworking, rearrangement (imbrication), and settling due to wave winnowing, resulting in a constant interplay between light exposure, surface abrasion, and burial. Many clasts become rapidly imbricated and buried in this dynamic environment, leading to a heterogeneous degree of bleaching among clasts and within the same cobble surface. Nevertheless, other clasts instead have time to be exposed to light, at least sufficiently to achieve complete surface bleaching. Imbrication, abrasion and attrition of soft cobbles may compete with luminescence resetting, consequently causing heterogeneous light exposure and shifting of the signal depth profile upward towards the rock surface (Liu et al., 2019). Moreover, when dealing with Middle to Late-Pleistocene samples (100–300 ka), an additional challenge arises wherein the residual luminescence signal may experience regrowth near saturation levels at the surface, with a consequence of complete or partial depletion of pre-burial bleaching front. Although a clear bleaching front is observable for cobbles that underwent a brief period of burial following an undisturbed prolonged bleaching phase (e.g., Smith et al., 2023), its evaluation becomes more intricate, and it is not straightforward for cobbles that had rapid transportation, shorter light exposition a longer period of burial (>100 ka). Therefore, the efficacy of the RSD method in dating gravelly lag deposits hinges on the clasts having a high probability of bleaching during transport and remaining undisturbed throughout burial.

6. Conclusions

The aim of this study was to assess the feasibility of OSL RSD of Pleistocene gravelly lag deposits in order to broaden the application range of this method. The method was applied to five cobbles belonging to a late Pleistocene (MIS 5e) transgressive gravelly lag at Cala Mosca site (Southern Sardinia).

We started from the awareness that suitability of RSD samples is based on the assumption that luminescence signal has been totally reset before burial. However, if the depositional environment is arduous for bleaching and even the samples are relatively old in age (>100 ka), to find a suitable surface may be challenging. The assessment of bleaching through the M/N ratio could be affected by several uncertainties that are worth investigating. This is also confirmed by the imprecise or failed fitting of several profiles.

Moreover, we found that by only focusing on the evaluation of the M/N ratio, the obtained ages were scattered and would not have led to a consistent and robust value if we had no confront independent age. To ensure that the results obtained were reliable we followed a systematic approach consisting of three acceptance criteria consecutive steps: a, b, c. These were applied on each analyzed core drilled from the cobbles. The analysis of the luminescence-depth profiles revealed that one cobble was sufficiently bleached prior to burial. This cobble yielded fading corrected $pIRIR_{225}$ and $pIR_{50/225}$ burial ages of 131 ± 8 ka and 127 ± 8 ka, respectively. These ages are consistent within the error limits and in agreement with the independent age control of ~130 ka based on U/Th dating of coral fragments and conventional luminescence dating of sand deposits. Given that the $pIRIR_{225}$ signal is more difficult to bleach than the $pIR_{50/225}$ signal, the agreement between the ages derived from the two signals suggests that the surface of cobble CLMr1 was sufficiently bleached prior to burial.

Confidence in complete resetting of luminescence signal before burial is a great advantage of OSL RSD. Our results indicate that, in environments where bleaching conditions are not optimal, the comparative analysis and the agreement of ages derived from different luminescence signals remains the most robust and valuable approach to assess the completeness of signals resetting prior to burial.

Finally, it is pertinent to acknowledge that the Rock Surface Dating (RSD) method continues to face challenges, such as a relatively high rate of samples rejection (80% of discharge for the studied cobbles) in comparison to the traditional methods. On the other hand, with the proposed three-steps methodology we are confident that the obtained ages could be considered reliable also in absence of independent absolute dating.

Funding

This work has been founded by the European Union Next-GenerationEU (PIANO NAZIONALE DI RIPRESA E RESILIENZA (PNRR) – MISSIONE 4 COMPONENTE 2, "Dalla ricerca all'impresa" INVESTIMENTO 1.4 – D.D. 1034 17/06/2022, CN00000033), SPOKE 1 "National Biodiversity Future Center - NBFC" and by "ACCORDO DI RICERCA TRA AUTORITA' DI SISTEMA PORTUALE DEL MARE DI SARDEGNA E UNIVERSITÀ DEGLI STUDI DI SASSARI, DIPARTIMENTO DI ARCHITETTURA, DESIGN E URBANISTICA (Poseidonia 2022, Resp. Prof. Vincenzo Pascucci)".

CRediT authorship contribution statement

Giulia Cossu: Writing – original draft, Visualization, Validation, Methodology, Investigation, Formal analysis, Data curation, Conceptualization. **Daniele Sechi:** Writing – review & editing, Supervision, Methodology, Investigation, Data curation, Conceptualization. **Reza Sohbati:** Writing – review & editing, Visualization, Validation, Supervision, Methodology, Data curation, Conceptualization. **Andrew Murray:** Supervision, Methodology, Conceptualization. **Vincenzo Pascucci:** Writing – review & editing, Supervision, Conceptualization. **Stefano Andreucci:** Writing – review & editing, Validation, Supervision, Data curation, Conceptualization.

Declaration of competing interest

The authors declare that they have no known competing financial interests or personal relationships that could have appeared to influence the work reported in this paper.

Data availability

Data will be made available on request.

Appendix A. Supplementary data

Supplementary data to this article can be found online at https://doi.org/10.1016/j.quageo.2024.101630.

References

Aitken, M.J., 1985. Thermoluminescence Dating. Academic Press, London.

al Khasawneh, S., Murray, A., Abudanah, F., 2019. A first radiometric chronology for the KhattShebib megalithic structure in Jordan using the luminescence dating of rock surfaces. Quat. Geochronol. 49, 205–210. https://doi.org/10.1016/j.quageo.2018.02.007.

Andreucci, S., Pistis, M., Funedda, A., Loi, A., 2017. Semi-isolated, flat-topped carbonate platform (Oligo-Miocene, Sardinia, Italy): sedimentary architecture and processes. Sediment. Geol. 361, 64–81. https://doi.org/10.1016/j.sedgeo.2017.09.012.

Barca, S., Melis, E., Annino, E., Cincotti, F., Ulzega, A., Orrù, P., Pintus, C., 2005. Note Illustrative della Carta Geologica d'Italia alla scala 1: 50.000, foglio 557. Cagliari: Servizio Geologico d'Italia. Carta Geologica d'Italia, scale 1 (10), 000.

Brennan, B.J., Lyons, R.G., Phillips, S.W., 1991. Attenuation of alpha particle track dose for spherical grains. Int. J. Radiat. Appl. and Instrum. Part D. Nuclear Tracks and Radiation Measurements 18 (1–2), 249–253.

Brill, D., Ageby, L., Obert, C., Hollerbach, R., Duval, M., Kolb, T., Bartz, M., 2021. Investigating the resetting of IRSL signals in beach cobbles and their potential for rock surface dating of marine terraces in Northern Chile. Mar. Geol. 443, 106692. https://doi.org/10.1016/j.margeo.2021.106692.

Buylaert, J.P., Murray, A.S., Thomsen, K.J., Jain, M., 2009. Testing the potential of an elevated temperature IRSL signal from K-feldspar. Radiat. Meas. 44 (5–6), 560–565.

Casini, L., Andreucci, S., Sechi, D., Huang, C.Y., Shen, C.C., Pascucci, V., 2020. Luminescence dating of Late Pleistocene faults as evidence of uplift and active tectonics in Sardinia, W Mediterranean. Terra. Nova 32 (4), 261–271. https://doi.org/10.1111/ter.12458.

Casula, G., Cherchi, A., Montadert, L., Murru, M., Sarria, E., 2001. The Cenozoic graben system of Sardinia (Italy): geodynamic evolution from new seismic and field data. Mar. Petrol. Geol. 18 (7), 863–888.

Chapot, M.S., Sohbati, R., Murray, A.S., Pederson, J.L., Rittenour, T.M., 2012. Constraining the age of rock art by dating a rockfall event using sediment and rock-surface luminescence dating techniques. Quat. Geochronol. 13, 18–25. https://doi.org/10.1016/j.quageo.2012.08.005.

Cocco, F., Andreucci, S., Sechi, D., Cossu, G., Funedda, A., 2019. Upper Pleistocene tectonics in western Sardinia (Italy): insights from the Sinis peninsula structural high. Terra. Nova 31, 485–493. https://doi.org/10.1111/ter.12418.

Cresswell, A.J., Carter, J., Sanderson, D.C.W., 2018. Dose rate conversion parameters: assessment of nuclear data. Radiat. Meas. 120, 195–201. https://doi.org/10.1016/j.radmeas.2018.02.007.

Cunningham, A.C., Murray, A.S., Armitage, S.J., Autzen, M., 2018. High-precision natural dose rate estimates through beta counting. Radiat. Meas. 120, 209–214. https://doi.org/10.1016/j.radmeas.2018.04.008.

Doglioni, C., Gueguen, E., Harabaglia, P., Mongelli, F., 1998. On the origin of W-directed subduction zones and applications to the western Mediterranean. In: Durand, B., Jolivet, L., Horvath, F., Séranne, M. (Eds.), The Mediterranean Basins: Tertiary Extension within the Alpine Orogen. Special Publication, Geol. Soc., London, pp. 541–561.

Ferranti, L., Burrato, P., Sechi, D., Andreucci, S., Pepe, F., Pascucci, V., 2021. Late Quaternary coastal uplift of southwestern Sicily, central Mediterranean sea. Quat. Sci. Rev. 255, 106812. https://doi.org/10.1016/j.quascirev.2021.106812.

Freiesleben, T., Sohbati, R., Murray, A., Jain, M., al Khasawneh, S., Hvidt, S., Jakobsen, B., 2015. Mathematical model quantifies multiple daylight exposure and burial events for rock surfaces using luminescence dating. Radiat. Meas. 81, 16–22. https://doi.org/10.1016/j.radmeas.2015.02.004.

Guérin, G., Mercier, N., Adamiec, G., 2011. Dose-rate conversion factors: update. Ancient Tl 29, 5–8.

Hearty, P., 1986. An inventory of last Interglacial (sensu lato) age deposits from the Mediterranean basin: a study of isoleucine epimerization and U- series dating. Zeitschrift fur Geomorphologie, Supplementband 62, 51–69.

Hoffmann, G., Schneider, B., Mechernich, S., Falkenroth, M., Dunai, T., Preusser, F., 2020. Quaternary uplift along a passive continental margin (Oman, Indian Ocean). Geomorphology 350, 106870. https://doi.org/10.1016/j.geomorph.2019.106870.

Huntley, D.J., Baril, M.R., 1997. The K content of the K-feldspars being measured in optical dating or in thermoluminescence dating. Ancient Tl 15, 11–13.

Ishii, Y., Takahashi, T., Ito, K., 2022. Luminescence dating of cobbles from Pleistocene fluvial terrace deposits of the Ara River, Japan. Quat. Geochronol. 67, 101228. https://doi.org/10.1016/j.quageo.2021.101228.

Kennedy, D.M., Stephenson, W.J., Naylor, L.A., 2014. Rocky Coast Geomorphology: a Global Synthesis. Geological Society Books, London.

Liu, J., Cui, F., Murray, A.S., Sohbati, R., Jain, M., Gao, H., Li, W., Li, C., Li, P., Zhou, T., Chen, J., 2019. Resetting of the luminescence signal in modern riverbed cobbles along the course of the Shiyang River, China. Quat. Geochronol. 49, 184–190. https://doi.org/10.1016/j.quageo.2018.04.004.

Muhs, D.R., Schumann, R.R., Groves, L.T., Simmons, K.R., Florian, C.R., 2021. The marine terraces of Santa Cruz Island, California: implications for glacial isostatic adjustment models of last-interglacial sea-level history. Geomorphology 389, 107826. https://doi.org/10.1016/j.geomorph.2021.107826.

Murray, A.S., Marten, R., Johnston, A., Martin, P., 1987. Analysis for naturally occurring radionuclides at environmental concentrations by gamma spectrometry. J. Radioanal. Nucl. Chem. 115 (2), 263–288.

Murray, A.S., Thomsen, K.J., Masuda, N., Buylaert, J.P., Jain, M., 2012. Identifying well-bleached quartz using the different bleaching rates of quartz and feldspar luminescence signals. Radiat. Meas. 47, 688–695. https://doi.org/10.1016/j.radmeas.2012.05.006.

Murray, A.S., Helsted, L.M., Autzen, M., Jain, M., Buylaert, J.P., 2018. Measurement of natural radioactivity: calibration and performance of a high-resolution gamma spectrometry facility. Radiat. Meas. 120, 215–220. https://doi.org/10.1016/j.radmeas.2018.04.006.

Oakley, D.O.S., Kaufman, D.S., Gardner, T.W., Fisher, D.M., VanderLeest, R.A., 2017. Quaternary marine terrace chronology, North Canterbury, New Zealand, using amino acid racemization and infrared-stimulated Luminescence. Quat. Res. (Tokyo) 87, 151–167. https://doi.org/10.1017/qua.2016.9.

Pascucci, V., Andreucci, S., Sechi, D., Casini, L., 2018. Late quaternary stratigraphy of western Sardinia (central mediterranean) based on luminescence age dating. Alp. and Mediterr. Quat. 31, 181–184.

Pasquetti, F., Bini, M., Giaccio, B., Ratti, A., Vacchi, M., Zanchetta, G., 2021. Chronology of the Mediterranean sea-level highstand during the Last Interglacial: a critical review of the U/Th-dated deposits. J. Quat. Sci. 36, 1174–1189. https://doi.org/10.1002/jqs.3359.

Pedoja, K., Husson, L., Johnson, M.E., Melnick, D., Witt, C., Pochat, S., Nexer, M., Delcaillau, B., Pinegina, T., Poprawski, Y., Authemayou, C., Elliot, M., Regard, V., Garestier, F., 2014. Coastal staircase sequences reflecting sea-level oscillations and tectonic uplift during the Quaternary and Neogene. Earth Sci. Rev. 132, 13–38. https://doi.org/10.1016/j.earscirev.2014.01.007.

Prescott, J.R., Hutton, J.T., 1994. Cosmic ray contributions to dose rates for Luminescence and ESR dating: large depths and long-term time variations. Radiat. Meas. 23, 497–500.

Rades, E.F., Sohbati, R., Lüthgens, C., Jain, M., Murray, A.S., 2018. First luminescence-depth profiles from boulders from moraine deposits: insights into glaciation chronology and transport dynamics in Malta valley, Austria. Radiat. Meas. 120, 281–289. https://doi.org/10.1016/j.radmeas.2018.08.011. Readhead, M. L., 2002. Absorbed dose fraction for 87Rb β particles. Ancient TL, 20(1), 25-28.

Readhead, M.L., 2002. Absorbed dose fraction for 87Rb β particles. Ancient TL 20 (1), 25–28.

Riedesel, S., Autzen, M., 2020. Beta and gamma dose rate attenuation in rocks and sediment. Radiat. Meas. 133, 106295. https://doi.org/10.1016/j.radmeas.2020.106295.

Saillard, M., Audin, L., Rousset, B., Avouac, J.-P., Chlieh, M., Hall, S.R., Husson, L., Farber, D.L., 2017. From the seismic cycle to long-term deformation: linking seismic coupling and Quaternary coastal geomorphology along the Andean megathrust. Tectonics 36, 241–256. https://doi.org/10.1002/2016TC004156.

Sechi, D., Andreucci, S., Stevens, T., Pascucci, V., 2020. Age and significance of late Pleistocene Lithophyllum byssoides intertidal algal ridge, NW Sardinia, Italy. Sediment. Geol. 400, 105618. https://doi.org/10.1016/j.sedgeo.2020.105618.

Sechi, D., Andreucci, S., Cocco, F., Pascucci, V., 2023. Stratigraphy and chronology of the Cala Mosca site, SW Sardinia (Italy). Quat. Res. 112, 160–179. https://doi.org/10.1017/qua.2022.45.

Simms, A.R., DeWitt, R., Kouremenos, P., Drewry, A.M., 2011. A new approach to reconstructing sea levels in Antarctica using optically stimulated Luminescence of cobble surfaces. Quat. Geochronol. 6 (1), 50–60.

Smedley, R.K., Pearce, N.J.G., 2016. Internal U, Th and Rb concentrations of alkali-feldspar grains: implications for luminescence dating. Quat. Geochronol. 35, 16–25. https://doi.org/10.1016/j.quageo.2016.05.002.

Smith, L.N., Sohbati, R., Jain, M., 2023. Rock surface luminescence dating of gravel determines the age of a glacial outburst megaflood, Glacial Lake Missoula, Montana, USA. Geology 51 (4), 323–328. https://doi.org/10.1130/G50721.1.

Sohbati, R., Murray, A.S., Jain, M., Buylaert, J.P., Thomsen, K.J., 2011. Investigating the resetting of OSL signals in rock surfaces. Geochronometria 38, 249–258. https://doi.org/10.2478/s13386-011-0029-2.

Sohbati, R., Murray, A.S., Porat, N., Jain, M., Avner, U., 2015. Age of a prehistoric "Rodedian" cult site constrained by sediment and rock surface luminescence dating techniques. Quat. Geochronol. 30, 90–99. https://doi.org/10.1016/j.quageo.2015.09.002.

Sohbati, R., Murray, A., Lindvold, L., Buylaert, J.P., Jain, M., 2017. Optimisation of laboratory illumination in optical dating. Quat. Geochronol. 39, 105–111. https://doi.org/10.1016/j.quageo.2017.02.010.

Souza, P.E., Sohbati, R., Murray, A.S., Kroon, A., Clemmensen, L.B., Hede, M.U., Nielsen, L., 2019. Luminescence dating of buried cobble surfaces from sandy beach ridges: a case study from Denmark. Boreas 48, 841–855. https://doi.org/10.1111/bor.12402.

Souza, P.E., Sohbati, R., Murray, A.S., Clemmensen, L.B., Kroon, A., Nielsen, L., 2021. Optical dating of cobble surfaces determines the chronology of Holocene beach ridges in Greenland. Boreas 50, 606–618. https://doi.org/10.1111/bor.12507.

Telesca, D., Longhitano, S.G., Pistis, M., Pascucci, V., Tropeano, M., Sabato, L., 2020. Sedimentology of a transgressive middle-upper Miocene succession filling a tectonically confined, current dominated seaway (the Logudoro Basin, northern Sardinia, Italy). Sediment. Geol. 400, 105626. https://doi.org/10.1016/j.sedgeo.2020.105626.

Thiel, C., Buylaert, J.P., Murray, A., Terhorst, B., Hofer, I., Tsukamoto, S., Frechen, M., 2011. Luminescence dating of the Stratzing loess profile (Austria)–Testing the potential of an elevated temperature post-IR IRSL protocol. Quat. Int. 234 (1–2), 23–31.

Zecchin, M., Catuneanu, O., Caffau, M., 2019. Wave-ravinement surfaces: classification and key characteristics. Earth Sci. Rev. 188, 210–239. https://doi.org/10.1016/j.earscirev.2018.11.011.